ACS OMEGA

Open Access



http://pubs.acs.org/journal/acsodf

Article

# Antifungal Activity of Electrochemically Etched Nanotextured Stainless Steel against *Candida albicans* and *Fusarium oxysporum* Fungal Cells

Anuja Tripathi, Cheick Dosso, and Julie A. Champion*

Cite This: *ACS Omega* 2025, 10, 19326−19334

Read Online

ACCESS | Metrics & More | Article Recommendations | Supporting Information

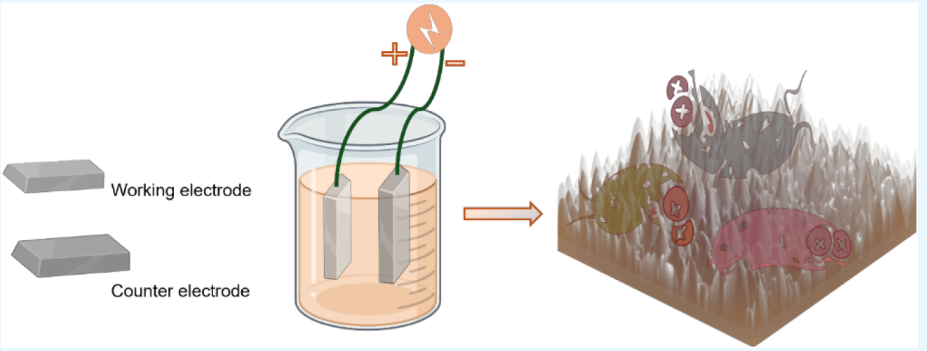


**ABSTRACT:** Fungal adhesion to stainless steel, an alloy commonly used in the food and beverage sectors, public and healthcare settings, and numerous medical devices, can give rise to serious infections, ultimately leading to morbidity, mortality, and significant healthcare expenses. In this study, we demonstrate that nanotextured stainless steel (nSS) fabricated using an electrochemical technique is an antibiotic-free biocidal surface against *Candida albicans* and *Fusarium oxysporum* fungal cells with 98% and 97% reduction, respectively. The nanoprotrusion features on nSS can have both physical contact with cell membranes and a chemical impact on cells through the production of reactive species; this material should not contribute to drug-resistant fungus as antibiotics can. As nSS is also antibacterial and compatible with mammalian cells, the demonstration of antifungal activity gives nSS the potential to be used to create effective, scalable, and sustainable solutions to broadly and responsibly prevent fungal and other microbial infections caused by surface contamination.

## INTRODUCTION

Fungal infections, as of January 2024, result in nearly 3.8 million deaths annually worldwide, nearly doubling the estimated 2 million deaths recorded in 2012.[1] The fungal pathogen *Candida albicans* caused >150 million mucosal infections and ∼200,000 deaths per year due to invasive and disseminated fungal infections in susceptible populations.[2,3] This significant increase highlights the formidable challenges in managing fungal diseases, especially in cases of weakened immune function. Fungal species can transform into aggressive pathogens, spreading throughout the body, and causing invasive fungal infections that may affect various organs and bodily systems. They can also colonize a wide range of surfaces, including paint coatings, cellulose-based materials, and stainless steel.[4−6] Likewise, species within the *Fusarium* genus, such as *Fusarium oxysporum*, have the potential to induce infections in immunocompromised patients, impacting different organs.[7] Despite significant research on bacterial adhesion,[8−10] little is known about the adhesion behaviors of *Candida* and *Fusarium* species. Thorough disinfection of healthcare facilities and tools helps address this issue. However, contamination can still occur and conventional antifungal drugs such as allylamines, azoles, echinocandins, 5-fluorocytosine, and polyenes can be highly irritating and toxic to humans and may foster drug resistance in microbes.[11−13]

In previous attempts to develop antifungal surfaces capable of repelling filamentous fungi, nanocomposites like hydrogenated carbon doped with copper using magnetron sputtering were developed.[14] However, the antifungal activity was effective only after copper was applied on graphite; graphite alone showed no antifungal properties. Some other approaches include coating chlorhexidine (an antifungal drug) onto nitride acrylonitrile butadiene styrene, grafting caspofungin (an antifungal drug) onto polymethacrylates, and poly(ethylene-

Received: October 18, 2024
Revised: March 31, 2025
Accepted: April 24, 2025
Published: May 7, 2025

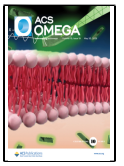

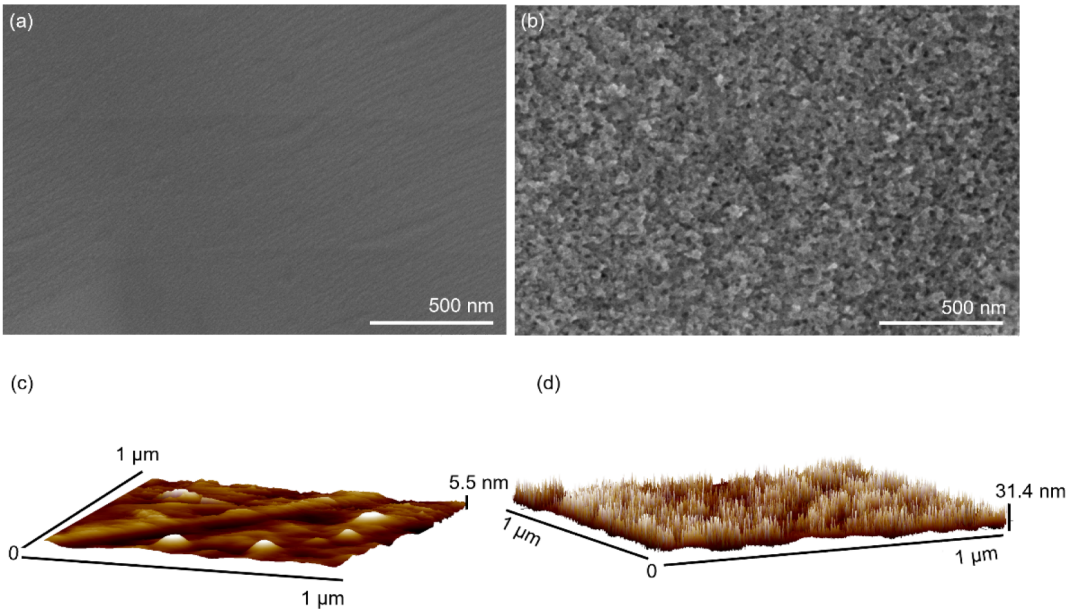


**Figure 1.** Scanning electron microscopy (a,b) and atomic force microscopy images (c,d) of pristine stainless steel (SS) (a,c) and nanotextured stainless steel (nSS) (b,d) etched for 30 s at 8 V.

*co*-vinyl alcohol) modified with carbendazim (a fungicide) (Antifungal effect of carbendazim supported on poly(ethylene-*co*-vinyl alcohol) and epoxy resin).[15−17] However, microbes may develop resistance against such biocides, posing a significant challenge. Nanotexturing may present a unique opportunity to develop surfaces that exhibit robust and long-lasting antifungal activity. For instance, Lee and Hwang fabricated a superhydrophobic aluminum/silicon surface that could reduce fungal contamination of industrial brazed aluminum heat exchangers.[18] The superhydrophobic surface was generated by the growth of hierarchical micronanostructures and the subsequent application of a hydrophobic polymer coating. Ivanova et al. reported plasma reactive ion etching for nanopillar silicon surfaces that inhibit fungal attachment through physical rupture.[19] Sampaio et al. developed a ZnO nanostructured thin film using glancing angle deposition for antifungal activity, reporting a 68% inhibition of viable cells.[20] Although these materials have shown effective antifungal properties, the feasibility of micro/nano-fabrication technologies is limited by complex fabrication processes, long processing times, a lack of practical applications, and high costs. Thus, it is essential to identify cost-effective, scalable nanofabrication methods and materials for widespread use in combating fungal infections resulting from surface contamination.

Stainless steel (SS) is frequently employed in communal environments, increasing the chances of infection transmission through items such as door handles, faucets, stethoscopes, and food storage containers. Vieira et al. demonstrated that stainless steel treated with a combination of nonthermal plasma and a diamond-like carbon coating using chemical vapor deposition exhibited antifungal activity against *Candida albicans*.[21] While SS itself lacks antimicrobial properties, adding nanotexture to SS can modify its properties, making it suitable for use as antimicrobial surfaces in healthcare. Our previous work showed the antibacterial properties of nanotextured stainless steel (nSS) using electrochemical etching against both Gram-positive and Gram-negative bacteria while being compatible with mammalian cells.[22,23] Electrochemical etching is already widely used industrially for electropolishing. As such, adaptation of voltage and time to create nSS requires minimal specialized equipment and can be scaled for larger surfaces, making it economically viable for industrial production.[24] However, the antifungal properties of nSS have not yet been investigated. In this work, we demonstrate for the first time the antifungal potential of nanotextured stainless steel with nanoprotrusion features that impede fungal attachment and proliferation. In addition to antimicrobial properties, nSS fabrication by electrochemical methods instead of nanofabrication renders it cost-effective, scalable, and tunable via factors such as the reaction time or voltage.

## RESULTS AND DISCUSSION

Nanotextured stainless steel (nSS) samples were created by etching SS316L stainless steel at 8 V for 30 s.[23] The resulting morphology, visible by scanning electron microscopy (SEM) and atomic force microscopy (AFM), compared to unmodified steel, is illustrated in Figure 1. The nSS surface shows nanopores evenly distributed, with a pore size ranging from 10 to 30 nm and vertical structures approximately 30 nm in height as measured by AFM, resembling the morphology achieved through cleanroom techniques. The SS (unmodified) surface appears notably smooth, with an average roughness of 3.2 ± 0.61 nm, while nSS has an average roughness of 25.3 ± 3.1 nm, which shows a similar morphology as cleanroom-developed fabrication techniques.[25,26] In our previous study,[23] the elemental composition and crystallinity of the SS and nSS were characterized using Fourier transform infrared spectroscopy (FTIR) and X-ray diffraction (XRD), indicating the absence of any functional groups and the austenite phase, respectively, for both materials. As a preliminary assessment of the mechanical properties of nSS, we used 640 g static weight for 15 min, as shown in Figure S1. The weight loading did not appear to damage or eliminate the nanostructures.

To investigate cell adhesion on steel surfaces, we conducted colony-forming unit (CFU) assays, SEM imaging, and growth



https://doi.org/10.1021/acsomega.4c09511
ACS Omega 2025, 10, 19326−19334

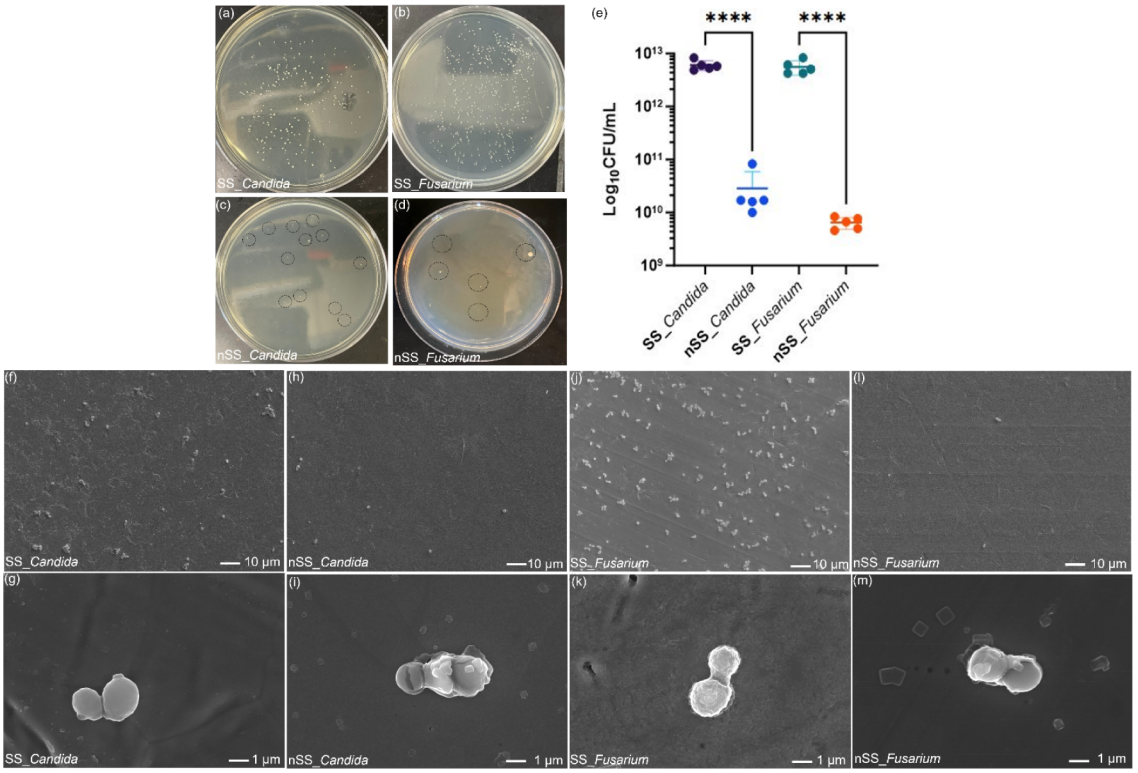


**Figure 2.** Colonies formed by cells recovered from SS and nSS samples after incubation for 24 h with *Candida* (a,c) and *Fusarium* (b,d). Representative $10^{-12}$ dilution plates are shown. The quantity of adhered cell number was characterized by counting CFU per sample (e). Data represent mean ± SD, $n = 3$, **** $p < 0.0001$. SEM images show the number and morphology of fungal cells adhered on SS (f, g, j, k) and nSS (h, i, l, m) surfaces after 24 h of culture.

curve analysis. Fungal cells collected from nSS surfaces showed significantly reduced growth compared to those from SS surfaces, with reductions of 98.0% for *Candida* and 96.8% for *Fusarium*, respectively (Figure 2). This lower fungal adhesion on nSS surfaces can be attributed to nanoprotrusion characteristics, which could reduce the adherence due to low accessible surface area or physically disrupt fungal cell membranes. In Figure 2f–m, SEM images also reveal that there are fewer total adhered cells on nSS than on SS for both *Candida* and *Fusarium*. No morphological alterations were observed in the cells adhered to SS, indicating the absence of cell damage. In contrast, cells on nSS showed some morphological changes. Kinetic growth assays reveal that SS supports the growth of both *Candida albicans* and *Fusarium oxysporum* after a lag phase (Figure S2). However, exposure to nSS inhibited their growth, leading to prolonged lag phases and lower OD600 values at the end of the growth period. These growth curve patterns are consistent with previously reported findings on the antifungal activities of transition metal complexes and Ni nanoparticles.[27,28]

We performed live/dead staining with fluorescence microscopy to investigate whether the nanoprotrusions on nSS induce fungal cell death or hinder their adhesion through repellent forces. Images in Figure 3a–h show a high live cell count and a low dead cell count for both fungi in contact with SS. In contrast, nSS surfaces had reduced live cells and an increased number of dead cells for both *Candida* and *Fusarium*, consistent with reduced CFU counts. To quantify fungal cell killing on steel surfaces, flow cytometry was used with propidium iodide (PI) staining, as shown in Figures 3i,j and S3 with untreated and peroxide-treated cells as controls. As expected, the percentage of dead cells collected from nSS samples was significantly larger than that from SS samples. While SS itself may induce a loss of cell viability due to exposure to trace amounts of iron in steel and inadequate nutrient supply,[29,30] nSS causes additional cellular damage. These results suggest that the nanoprotrusive features of nSS surfaces exert mechanical stress on the membranes of adhered fungi, resulting in membrane damage and cell death.

In addition to decreased viability, flow cytometry also revealed significant changes in fungal populations upon analysis of the forward scattering (FSC) and side scattering (SSC) of cells. Figure 4 a,d shows two distinct populations of healthy fungi labeled as P3 and P4. P4 corresponds to budding cells and microconidia in *Candida* and *Fusarium*, respectively, which are actively engaged in cellular division and proliferation and make up about a third of the total population.[32−34] Optical images of budding cells from untreated cells after overnight culture are presented in Figure S4. P3 comprises nonbudding cells and macroconidia for *Candida* and *Fusarium*, respectively, which can be multicellular, environmentally resistant, exhibit low metabolic activity, and propagate slowly.[35−39] Incubation with both SS and nSS drastically reduced the number of budding cells, or microconidia (Figure 4a–h). For *Candida* nSS further reduced the budding population from SS, but essentially no *Fusarium* were collected from either SS or nSS. This indicates that either budding/microconidia do not bind significantly to steel or that steel itself affects budding/microconidia cells. As some of the metals in steel, such as iron, are both essential for life and toxic, depending on the concentration,[40] budding cells may be more sensitive to steel surfaces than nonbudding cells. Additionally, the number of



https://doi.org/10.1021/acsomega.4c09511
ACS Omega 2025, 10, 19326−19334

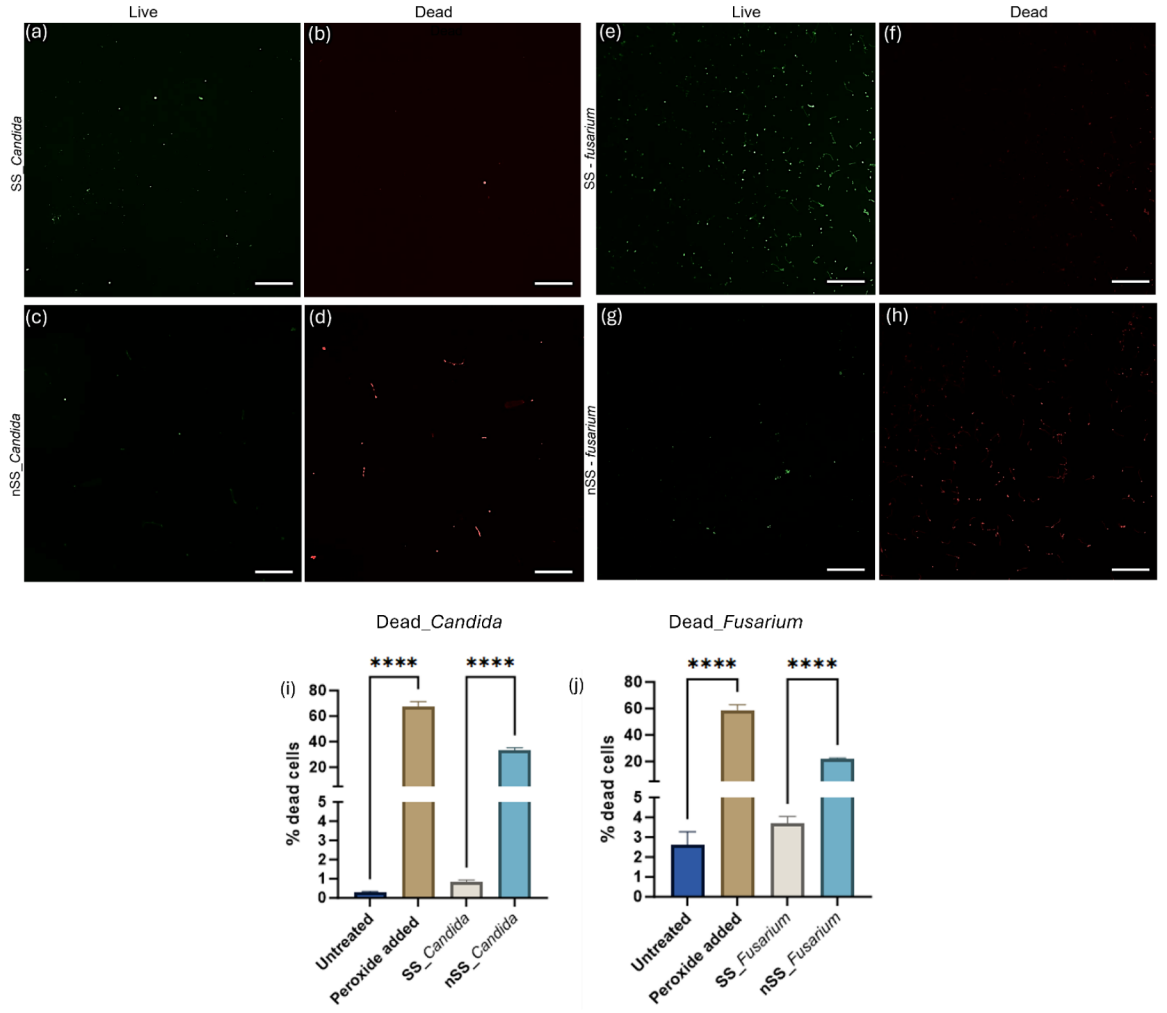


**Figure 3.** Representative fluorescent micrographs of *Candida* (a–d) and *Fusarium* (e–h) cells cultured for 24 h on pristine stainless steel (a–f) and nanotextured stainless steel (c,d,g,h) surfaces. The brightness and sharpness of these images were uniformly adjusted to improve visual clarity. Samples were stained using SYTO 9 and PI, respectively, for live (green) and dead (red) fungal cells. All scale bars are 30 $\mu$m. Percentage of dead *Candida* (i) and *Fusarium* (j) labeled with propidium iodide after incubating 24 h with peroxide, SS and nSS. Data represented here as mean ± SD, **** $p \leq 0.0001$. It should be noted that a small fraction of cells (<10%) that label with PI are not dead and can recover from the stress.[31]

nonbudding or macroconidia populations increased on both steel surfaces (Figure 4i,j), suggesting that some cells might have transitioned from budding/microconidia to a reduced metabolic activity state.

To identify the mechanism of nSS fungal killing, we conducted membrane depolarization analysis using DiOC2 (3,3′-diethyoxacarbocyanineiodide) dye and CCCP (carbonyl cyanide *m*-chlorophenyl hydrazone) treated positive control cells. The DiOC2 dye emits green fluorescence in cells, but as the dye molecules self-associate due to higher cytosolic concentrations caused by disrupted membrane potential, the fluorescence shifts to red emission. As shown in Figure S5, fungal cells incubated with SS or nSS did not exhibit any evidence of membrane depolarization. To assess if nSS induced fungal stress in the form of intracellular reactive oxygen species (ROS) generation, which was observed for bacteria,[23] we used flow cytometry to measure dichlorodihydrofluorescein diacetate (DCFDA) in fungal cells. Untreated and peroxide-treated fungal cells served as negative and positive controls. The peroxide controls and SS/nSS-incubated fungal samples showed that only budding or microconidia cells demonstrate the ROS response (Figure S6). Figure 5 summarizes the data, and though very few budding cells were collected from either steel surface, a small increase in ROS for budding *Candida* was observed for cells incubated with nSS compared to untreated cells or SS incubation. In contrast, no evidence of ROS production was observed in the small microconidia population of *Fusarium*, possibly due to the strain's high adaptation to oxidative stress.[41] Notably, molecular dynamics simulation results from bacterial studies offer valuable insights, showing that 10 nm high nanopillars can induce localized stresses on the cell membrane.[42] These stresses can deform the membrane, ultimately leading to rupture or membrane withdrawal. Although yeast cell membranes differ structurally from bacteria, similar stress concentrations could arise within the fungal cell wall or plasma membrane in response to mechanical forces or nanoprotrusion-induced pressure.

During cellular apoptosis, ROS generation initiates mitochondrial dysfunction, leading to mitochondrial membrane depolarization and the translocation of proapoptotic factors such as cytochrome c (CytC). In Figure 6, the levels of CytC within the mitochondria of all cells were measured. Cells incubated with SS showed normal CytC levels in mitochondria, whereas *Candida* cells exposed to nSS exhibited modestly


https://doi.org/10.1021/acsomega.4c09511
ACS Omega 2025, 10, 19326−19334

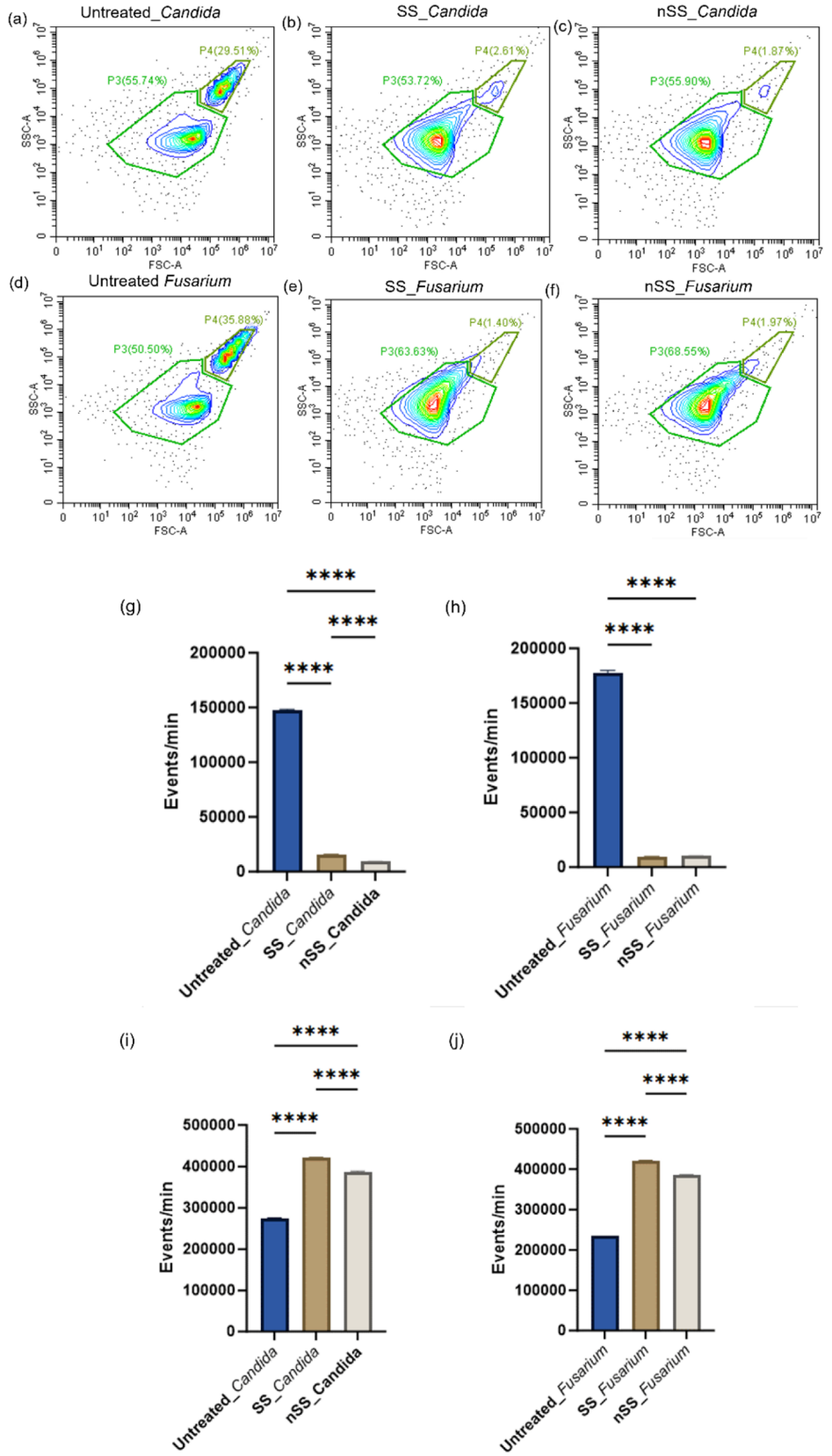


**Figure 4.** Cell size (forward scatter, FSC) and granularity (side scatter, SSC) were assessed via flow cytometry after incubation in control liquid culture (untreated) or with SS and nSS surfaces for 24 h (a−f). P4 corresponds to microconidia or budding yeast, while P3 represents macroconidia or nonbudding yeast. The frequency of P4 and P3 after 24 h of incubation in SS and nSS is represented as (g,h) and (i,j), respectively. Data represented here as mean ± SD, $n = 3$, **** $p \leq 0.0001$ (one way ANOVA).



https://doi.org/10.1021/acsomega.4c09511
*ACS Omega* 2025, 10, 19326−19334

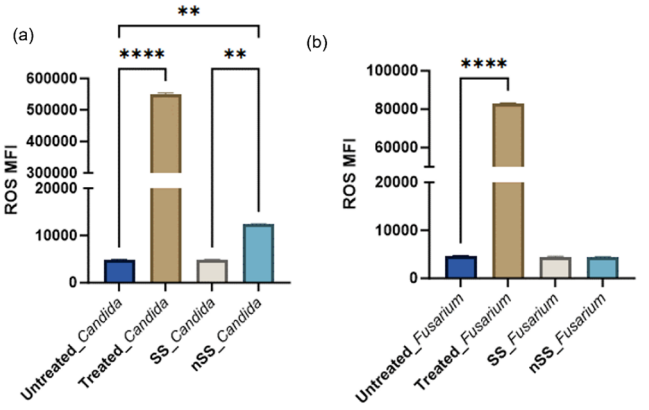


**Figure 5.** Mean fluorescence intensity (MFI) of *Candida* (a) and *Fusarium* (b) cells labeled for intracellular ROS using the dye DCFDA. Increased fluorescence indicates increased levels of ROS. Cells were incubated with steel surfaces or hydrogen peroxide (treated) for 24 h. Data are presented from three independent experiments using the mean ± SD ($n$ = 3, $^{**}p < 0.01$, $^{****}p < 0.0001$, one way ANOVA).

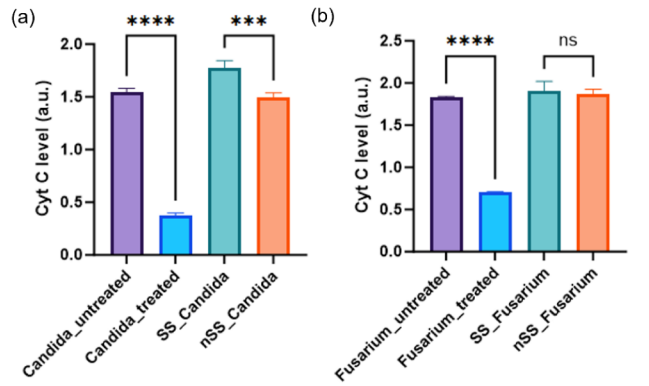


**Figure 6.** Cyt C in mitochondria was quantified in *Candida* (a) and *Fusarium* cells (b) treated with peroxide as positive control, SS and nSS. Data are presented from three independent experiments using the mean ± SD ($n$ = 3, $^{***}p < 0.005$, $^{****}$ $p < 0.000$).

reduced mitochondrial CytC levels, likely due to mitochondrial membrane damage and disruption of the electron transport chain. In contrast, no change in CytC release was observed in *Fusarium* when exposed to nSS or SS, consistent with the ROS study in Figure 5. This suggests potential differences in cellular physiology, metabolism, and genetic characteristics between these fungal cells, which may account for the variations in the mechanism of response to nSS between *Candida* and *Fusarium* fungal cells.[43−46]

## CONCLUSION

We have demonstrated the antifungal activity of nanotextured stainless steel developed by electrochemical etching featuring nanopores and nanoprotrusions. Although fungi exhibit a reduced presence of budding cells on steel surfaces, they can grow on steel and contaminate it. The nanotexture both reduced fungal cell adhesion and killed adherent cells, perhaps due to physical damage to the membrane as there was no evidence for large stress responses in the cells, although additional mechanistic studies are needed to provide direct proof of the mechanism. These findings align with a previous report on Ti surfaces with 50 nm sharp peaks, which repelled *Candida albicans* adhesion.[47] The electrochemical etching method for steel modification presented here has significant potential for practical use, as it offers a method to prevent fungal and bacterial adhesion and surface contamination without antibiotics that contribute to drug resistance. The cost-effectiveness and scalability of this surface modification approach make it practically relevant for larger-scale surfaces in public or healthcare settings. A limitation of this study is that it focused solely on two types of fungal cells, *Candida albicans* and *Fusarium oxysporum*. It did not include investigations into their spores, hyphae, or biofilms. Furthermore, experiments were conducted under controlled laboratory conditions, which may not fully reflect real-world environments, where factors like biofilm formation, fouling, and complex media play a role. At least in the short term, protein adsorption from the rich media did not inhibit antifungal activity. We have previously evaluated the adsorption of human serum proteins on nSS compared to SS and found differences in both the mass and identity of adsorbed proteins.[48] Future research could address these limitations by evaluating the nSS stability under mechanical abrasion, biofouling, and chemical exposure. Additionally, exploring nSS efficacy against a broader spectrum of fungal species—including filamentous fungi and biofilms—could yield results that inform biomedical applications, especially for implants, where infections remain a significant clinical challenge. Ivanova et al. demonstrated that Ti surfaces with sharp nanoscale peaks restricted *Candida albicans* to its yeast form, preventing biofilm formation and the transition to hyphal cells even after prolonged incubation.[47] Future experiments will reveal if electrochemically etched steel with a similar topography exhibits the same response as Ti.

## EXPERIMENTAL SECTION

**Materials.** Nitric acid (ACS reagent, 70%) and steel plates (30 × 20 × 0.05 $cm^3$) were purchased from Sigma-Aldrich and Maudlin Products, respectively. Insulating tape (Electroplating Tape 470) was purchased from 3M. Organic solvents acetone (99.5%), methanol (99.8%), and isopropanol (99.5%) were purchased from VWR International. Propidium iodide dye, DCFDA dye, and SYTO9 dye were purchased from Invitrogen. *Candida albicans* (18804) and *Fusarium oxysporum* (48112) were purchased from ATCC.

**Steel Sample Preparation.** Two SS316L steel samples of different sizes (2.5 × 1.5 × 0.05 and 2.5 × 2.5 × 0.05 $cm^3$) were cut in a machine shop. These samples were designated as the working and counter electrodes, respectively. The samples were sonicated for 7 min each in acetone, methanol, and isopropyl alcohol to eliminate organic contaminants. The samples were rinsed with water to remove organic solvents, followed by drying at ambient temperature. A stainless-steel wire was welded onto the SS316L samples to establish electrical connections to the cathode counter electrode. The working electrode was prepared using insulated tape to attach the wire, leaving an active area of 1 ± 0.06 $cm^2$ for electrochemical surface modification. A diluted nitric acid solution (48 wt %) was used as an electrolyte (caution! use personal protective equipment and do not mix nitric acid with organics). The separation distance between the working and counter electrodes was 6 cm. Electrochemical etching was done using a direct power source at 8 V for 30 s. After electrochemical etching, the steel samples were extracted from the electrochemical cell, rinsed with deionized water, and left


https://doi.org/10.1021/acsomega.4c09511
ACS Omega 2025, 10, 19326−19334

to air-dry at room temperature before being subjected to further characterization.

**Surface Characterization.** The surface morphologies of steel samples were analyzed by using scanning electron microscopy (SEM) with a Hitachi SU8230 instrument at a 3 kV acceleration potential. Pore sizes on SEM images were measured using imageJ software. Additionally, topographical information was gathered using atomic force microscopy (AFM, Bruker) and using AppNano ACT tapping mode AFM probes from Applied Nanosciences. The surface roughness parameters of steel samples were determined via AFM measurements, scanning a surface area of 1 $\mu m^2$, while avoiding artificial defect areas. Quantitative data on the mean roughness (Ra) and the root-mean-square (RMS) roughness (Rq) were extracted through image processing by using the AFM software. For the mechanical test, a 640 g steel block was carefully placed on the nSS samples for 15 min, followed by washing and SEM.

**Fungus Cell Cultures and Assays.** *Candida albicans* and *Fusarium oxysporum* cells were used in this study as model microorganisms. Steel samples were sterilized by an autoclave (15 psi, 121 °C for 20 min). The samples were then masked with tape to expose only the nanotextured part. Following the masking, the samples were sprayed with ethanol to ensure thorough sterilization and allowed to air-dry. Subsequently, the samples were transferred into 6-well cell culture plates and incubated with 5 mL of fungal solution (OD 0.3) in potato dextrose media for both fungi. Fungal cells were cultured on the samples for 24 h in an incubator (30 °C). To quantify the number of *Candida* and *Fusarium* cells adhered to each steel surface, the colony-forming units (CFUs) of adhered cells were counted using the spread plate method. At the end of the incubation, samples were initially washed with phosphate-buffered saline (PBS). The tape was then carefully removed with tweezers, followed by rinsing the samples five times with PBS and transferring them into a 50 mL tube with 5 mL of fresh PBS. Each sample was sonicated for 7 min and vortexed for 20 s to release the fungus remaining on the sample surface into the solution. The initial dilution was made by transferring 25 $\mu$L of the resuspended cell solution into 225 $\mu$L of fresh PBS and a series of 10-fold dilutions ($10^{-1}$−$10^{-12}$) in PBS was prepared in 96-well plates. Then, 30 $\mu$L of each diluted solution was spread onto potato dextrose agar plates by using sterile glass beads. Fungal colonies were counted after 24 h of incubation at 30 °C. The number of colonies (CFU) per sample was calculated by dividing the number of colonies by the dilution factor ($10^{-12}$) multiplied by the amount of cell suspension plated to agar (30 $\mu$L), then multiplying by the initial volume of cell suspension (5 mL).

To visualize cell adhesion on the surfaces using scanning electron microscopy (SEM), steel samples underwent preparation and incubation in a fungal cell solution as described above. After the incubation period, the steel samples were gently washed with PBS three times and then fixed with 2.5% glutaraldehyde at room temperature for 1 h. Following fixation, the samples underwent dehydration using a series of ethanol concentrations in distilled water (50%, 70%, 90%, and 100% ethanol) for 20 min each. The dehydrated samples were then dried overnight using hexamethyldisilazane (HMDS, Aldrich). Subsequently, the samples were sputter-coated with gold (approximately 7 nm thickness) using a Quorum Q-150T ES Sputter Coater. Surface morphologies of the SS316L samples were examined using a Hitachi SEM SU8010 instrument with a 3 kV acceleration potential.

**Confocal Laser Scanning Microscopy for Fungal Viability Assay.** To evaluate both cell viability and adhesion during the early stages of interaction, steel samples were prepared and immersed in fungal solution as described above for 24 h. Subsequently, the samples were washed with PBS and stained using the Live/Dead BacLight Bacterial Viability Kit (Life Technologies) for fluorescence microscopy analysis. Equal volumes of 3.34 mM SYTO9 (green dye for live cells) and 20 mM propidium iodide (red dye for dead cells) were combined in 1 mL of PBS. The staining solution was applied to each sample and allowed to incubate in the dark at room temperature for 15 min. Following incubation, the samples were placed upside down onto a glass slide and imaged with a 20× objective using a Nikon-C2 laser scanning confocal microscope. Live fungal cells were visualized using 488 nm laser excitation with a 525/50 nm emission filter, while dead fungal cells were visualized using 561 nm laser excitation with a 595/50 nm emission filter. The brightness and sharpness of the images were uniformly adjusted to improve visual clarity.

**Flow Cytometry for Membrane Depolarization, ROS, and Dead Cells Analysis.** To evaluate the impact of steel on the fungal cells, the cells were incubated on metal surfaces as described previously for 24 h. Subsequently, the metal surfaces were washed with 1 mL of PBS before the tape was removed, followed by washing with an additional 3 mL of PBS to remove any unbound fungus. After washing, 3 $\mu$L of 50 $\mu$M propidium iodide dye in 200 $\mu$L of PBS was added to investigate the dead cell population. 3 $\mu$L of 1 mM DCFDA dye in 1× buffer and 5 $\mu$L of 10 $\mu$M DiOC2 were added for ROS evaluation (ab113851, Abcam) and membrane depolarization (B34950, Thermo Fisher) studies, respectively. After a 30−45 min incubation period at 30 °C, the samples were scraped to detach the fungal cells, which were collected in 200 $\mu$L of PBS. The detached cells were then loaded onto a 96-well plate. Following an additional 45 min incubation at 30 °C, the cells were analyzed using a Cytoflex flow cytometer (Beckman Coulter) equipped with PE (phycoerythrin, 565 nm/574 nm) and FITC (fluorescein isothiocyanate, 498 nm/517 nm) channels. Untreated fungal cells served as the negative control, and cells treated with 1 $\mu$L of 50 mM CCCP and 1 $\mu$L of 50 mM peroxide were used as the positive control.

**Assessment of Cytochrome C Release.** *Candida* and *Fusarium* cells were incubated at 30 °C with metal samples for 24 h as described above or with 1 mM $H_2O_2$ for 4 h. Following the incubation period, metal surfaces were washed with 1 mL of PBS, and the cells that adhered to the metal surface were scraped. The collected cells were homogenized by vortexing with glass beads in buffer A (50 mM Tris, 2 mM EDTA, and 1 mM phenylmethylsulfonyl fluoride, pH 7.5). The resulting mixture was centrifuged at 2000 *g* for 10 min to obtain pellets. To isolate pure mitochondria, the pellet was washed in buffer B (50 mM Tris, 2 mM EDTA, pH 5.0) by centrifugation at 5000 *g* for 30 s. The mitochondria were then collected and suspended in Tris−EDTA buffer at a concentration of 2 mg/mL. After treatment with 500 mg/mL ascorbic acid for 5 min, the cytochrome c contents in the mitochondrial samples were measured at 550 nm using a plate reader (Synergy 2, Multimode Microplate Reader, BioTek).

**Statistical Analysis.** All fungal cell experiments were performed in triplicate. All data plotted with error bars represent mean values ± the standard deviation. One-way



https://doi.org/10.1021/acsomega.4c09511
ACS Omega 2025, 10, 19326−19334

ANOVA was performed to determine the statistical differences between the groups. Statistical significance was denoted as follows: * for $p \leq 0.05$, *** for $p \leq 0.001$, and **** for $p \leq 0.0001$. All statistical analyses were conducted using GraphPad Prism 10.

## ■ ASSOCIATED CONTENT

### Supporting Information

The Supporting Information is available free of charge at https://pubs.acs.org/doi/10.1021/acsomega.4c09511.

Mechanical test, flow cytometry analysis for dead cells, membrane depolarization, and ROS measurement, and fungal growth curves (PDF)

## ■ AUTHOR INFORMATION


### Corresponding Author

**Julie A. Champion** − *School of Chemical and Biomolecular engineering, Georgia Institute of Technology, Atlanta, Georgia 30332, United States;* orcid.org/0000-0002-0260-9392; Email: julie.champion@chbe.gatech.edu

### Authors

**Anuja Tripathi** − *School of Chemical and Biomolecular engineering, Georgia Institute of Technology, Atlanta, Georgia 30332, United States;* orcid.org/0000-0002-0950-1763

**Cheick Dosso** − *School of Chemical and Biomolecular engineering, Georgia Institute of Technology, Atlanta, Georgia 30332, United States;* Present Address: Department of Chemical Engineering, Carnegie Mellon University, Doherty Hall, 5000 Forbes Avenue, Pittsburgh, PA 15213, USA

Complete contact information is available at: https://pubs.acs.org/10.1021/acsomega.4c09511


### Notes

The authors declare no competing financial interest.

## ■ ACKNOWLEDGMENTS

This study was financially supported by Anuja Tripathi's Presidential Postdoctoral Fellowship at the Georgia Institute of Technology. We acknowledge Soomin Lee's assistance with the material preparation and Thomas Pho for guidance. This work was performed in part at the Georgia Tech Institute for Electronics and Nanotechnology, a member of the National Nanotechnology Coordinated Infrastructure, which is supported by the National Science Foundation (Grant No. ECCS-2025462). This work also used core facilities of the Petit Institute of Bioengineering and Biosciences at Georgia Tech. We are thankful to Bradley Parker for his kind help with cutting steel pieces for this study.

## ■ REFERENCES


(1) Denning, D. W. Global Incidence and Mortality of Severe Fungal Disease. *Lancet Infect. Dis.* **2024**, *24* (7), No. E428−E438.

(2) Richardson, J. P. Candida Albicans: A Major Fungal Pathogen of Humans. *Pathogens* **2022**, *11* (4), 459.

(3) Boretti, A. Steroids Induced Black Fungus Infection in India During the May 2021 COVID-19 Outbreak. *Indian J. Otolaryngol. Head Neck Surg.* **2022**, *74* (Suppl S2), 3216−3219.

(4) Joshi, M. H.; Balamurugan, P.; Venugopalan, V. P.; Rao, T. S. Dense Fouling in Acid Transfer Pipelines by an Acidophilic Rubber Degrading Fungus. *Biofouling* **2011**, *27* (6), 621−629.

(5) Guiamet, P.; Borrego, S.; Lavin, P.; Perdomo, I.; de Saravia, S. G. Biofouling and Biodeterioration in Materials Stored at the Historical Archive of the Museum of La Plata, Argentine and at the National Archive of the Republic of Cuba. *Colloids Surf., B* **2011**, *85* (2), 229−234.

(6) Pagano, L.; Mayor, S. Invasive Fungal Infections in High-Risk Patients: Report from TIMM-8 2017. *Future Sci. OA* **2018**, *4* (6), FSO307.

(7) Nucci, M.; Anaissie, E. Fusarium Infections in Immunocompromised Patients. *Clin. Microbiol. Rev.* **2007**, *20* (4), 695−704.

(8) Li, X.; Wu, B.; Chen, H.; Nan, K.; Jin, Y.; Sun, L.; Wang, B. Recent Developments in Smart Antibacterial Surfaces to Inhibit Biofilm Formation and Bacterial Infections. *J. Mater. Chem. B* **2018**, *6* (26), 4274−4292.

(9) Cloutier, M.; Mantovani, D.; Rosei, F. Antibacterial Coatings: Challenges, Perspectives, and Opportunities. *Trends Biotechnol.* **2015**, *33* (11), 637−652.

(10) Linklater, D. P.; Baulin, V. A.; Juodkazis, S.; Crawford, R. J.; Stoodley, P.; Ivanova, E. P. Mechano-Bactericidal Actions of Nanostructured Surfaces. *Nat. Rev. Microbiol.* **2021**, *19* (1), 8−22.

(11) Chaudhary, R. J.; Rathod, S. P.; Jagati, A.; Zankat, D.; Brar, A. K.; Mahadevia, B. Oral Antifungal Therapy: Emerging Culprits of Cutaneous Adverse Drug Reactions. *Indian Dermatol. Online J.* **2019**, *10* (2), 125−130.

(12) Castellsague, J.; García-Rodríguez, L.-A.; Duque, A.; Pérez, S. Risk of Serious Skin Disorders among Users of Oral Antifungals: A Population-Based Study. *BMC Dermatol.* **2002**, *2* (1), 14.

(13) Wei, C.-Y.; Michael Lee, M.-T.; Chen, Y.-T. Pharmacogenomics of Adverse Drug Reactions: Implementing Personalized Medicine. *Hum. Mol. Genet.* **2012**, *21* (R1), R58−R65.

(14) Ivanov-Omskii, V. I.; Panina, L. K.; Yastrebov, S. G. Amorphous Hydrogenated Carbon Doped with Copper as Antifungal Protective Coating. *Carbon* **2000**, *38* (4), 495−499.

(15) Watson, R.; Maxwell, M.; Dunn, S.; Brooks, A.; Jiang, L.; Hill, H. J.; Williams, G.; Kotowska, A.; Nikoi, N. D.; Stamataki, Z.; Banzhaf, M.; Scurr, D.; Bryant, J. A.; de Cogan, F. Development of Biocide Coated Polymers and Their Antimicrobial Efficacy. *Nano Sel.* **2023**, *4* (7), 442−453.

(16) Alex, J.; González, K.; Kindel, T.; Bellstedt, P.; Weber, C.; Heinekamp, T.; Orasch, T.; Guerrero-Sanchez, C.; Schubert, U. S.; Brakhage, A. A. Caspofungin Functionalized Polymethacrylates with Antifungal Properties. *Biomacromolecules* **2020**, *21* (6), 2104−2115.

(17) Park, E.-S.; Lee, H.-J.; Park, H. Y.; Kim, M.-N.; Chung, K.-H.; Yoon, J.-S. Antifungal Effect of Carbendazim Supported on Poly(Ethylene-Co-Vinyl Alcohol) and Epoxy Resin. *J. Appl. Polym. Sci.* **2001**, *80* (5), 728−736.

(18) Lee, J.-W.; Hwang, W. Exploiting the Silicon Content of Aluminum Alloys to Create a Superhydrophobic Surface Using the Sol−Gel Process. *Mater. Lett.* **2016**, *168*, 83−85.

(19) Linklater, D. P.; Le, P. H.; Aburto-Medina, A.; Crawford, R. J.; Maclaughlin, S.; Juodkazis, S.; Ivanova, E. P. Biomimetic Nanopillar Silicon Surfaces Rupture Fungal Spores. *Int. J. Mol. Sci.* **2023**, *24* (2), 1298.

(20) Pereira-Silva, P.; Costa-Barbosa, A.; Costa, D.; Rodrigues, M. S.; Carvalho, P.; Borges, J.; Vaz, F.; Sampaio, P. Antifungal Activity of ZnO Thin Films Prepared by Glancing Angle Deposition. *Thin Solid Films* **2019**, *687*, 137461.

(21) de Oliveira, S. M. M.; da Silva, N. S.; Sene, A.; Gandra, R. F.; Junges, D. S. B.; Ramos, M. A. R.; Vieira, L. Comparative Study of *Candida Albicans* Inactivation by Nonthermal Plasma on Stainless Steel with and without Diamond-like Carbon Film. *ACS Omega* **2019**, *4* (4), 6891−6902.

(22) Jang, Y.; Choi, W. T.; Johnson, C. T.; García, A. J.; Singh, P. M.; Breedveld, V.; Hess, D. W.; Champion, J. A. Inhibition of Bacterial Adhesion on Nanotextured Stainless Steel 316L by Electrochemical Etching. *ACS Biomater. Sci. Eng.* **2018**, *4* (1), 90−97.

(23) Tripathi, A.; Park, J.; Pho, T.; Champion, J. A. Dual Antibacterial Properties of Copper-Coated Nanotextured Stainless Steel. *Small* **2024**, *20* (38), 2311546.

(24) Shin, H.; Lee, S.; Sung, Y.-E. Industrial-Scale H2O2 Electrosynthesis in Practical Electrochemical Cell Systems. *Curr. Opin. Electrochem.* **2023**, *38*, 101224.
(25) Beena Unni, A.; Winkler, R.; Duarte, D. M.; Chat, K.; Adrjanowicz, K. Influence of Surface Roughness on the Dynamics and Crystallization of Vapor-Deposited Thin Films. *J. Phys. Chem. B* **2022**, *126* (40), 8072−8079.
(26) Ciambriello, L.; Cavaliere, E.; Gavioli, L. Influence of Roughness, Porosity and Grain Morphology on the Optical Properties of Ultrathin Ag Films. *Appl. Surf. Sci.* **2022**, *576*, 151885.
(27) Jeyaraj Pandian, C.; Palanivel, R.; Dhanasekaran, S. Screening Antimicrobial Activity of Nickel Nanoparticles Synthesized Using *Ocimum Sanctum* Leaf Extract. *J. Nanopart.* **2016**, *2016*, 4694367.
(28) Wani, M. Y.; Ahmad, A.; Malik, M. A.; Sobral, A. J. F. N. Mononuclear Transition Metal Complexes Containing Iodo-Imidazole Ring Endowed with Potential Anti-Candida Activity. *Med. Chem. Res.* **2016**, *25* (11), 2557−2566.
(29) B, A. W. Oligodynamic Phenomena of Living Cells. *Nature* **1893**, *48* (1240), 331.
(30) Santo, C. E.; Lam, E. W.; Elowsky, C. G.; Quaranta, D.; Domaille, D. W.; Chang, C. J.; Grass, G. Bacterial Killing by Dry Metallic Copper Surfaces. *Appl. Environ. Microbiol.* **2011**, *77* (3), 794−802.
(31) Davey, H. M.; Hexley, P. Red but Not Dead? Membranes of Stressed *Saccharomyces Cerevisiae* Are Permeable to Propidium Iodide. *Environ. Microbiol.* **2011**, *13* (1), 163−171.
(32) Mayer, F. L.; Wilson, D.; Hube, B. *Candida Albicans* Pathogenicity Mechanisms. *Virulence* **2013**, *4* (2), 119−128.
(33) Maheshwari, R. Microconidia OfNeurospora Crassa. *Fungal Genet. Biol.* **1999**, *26* (1), 1−18.
(34) Berman, J.; Sudbery, P. E. Candida Albicans: A Molecular Revolution Built on Lessons from Budding Yeast. *Nat. Rev. Genet.* **2002**, *3* (12), 918−931.
(35) Hatzis, C.; Porro, D. Morphologically-Structured Models of Growing Budding Yeast Populations. *J. Biotechnol.* **2006**, *124* (2), 420−438.
(36) Moreno-Sabater, A.; Autaa, G.; Sterlin, D.; Jerbi, A.; Villette, R.; Holm, J. B.; Parizot, C.; Selim, S.; Senghor, Y.; Ghillani-Dalbin, P.; Bachmeyer, C.; Hennequin, C.; Gorochov, G.; Larsen, M. Systemic Anti-Commensal Response to Fungi Analyzed by Flow Cytometry Is Related to Gut Mycobiome Ecology. *Microbiome* **2020**, *8* (1), 159.
(37) Sudbery, P. E. Growth of Candida Albicans Hyphae. *Nat. Rev. Microbiol.* **2011**, *9* (10), 737−748.
(38) Lin, X.; Alspaugh, J. A.; Liu, H.; Harris, S. Fungal Morphogenesis. *Cold Spring Harb. Perspect. Med.* **2015**, *5* (2), a019679.
(39) Brown, A. J. P.; Gow, N. A. R. Regulatory Networks Controlling Candida Albicans Morphogenesis. *Trends Microbiol.* **1999**, *7* (8), 333−338.
(40) Bird, A. J. Cellular Sensing and Transport of Metal Ions: Implications in Micronutrient Homeostasis. *J. Nutr. Biochem.* **2015**, *26* (11), 1103−1115.
(41) Ponts, N.; Couedelo, L.; Pinson-Gadais, L.; Verdal-Bonnin, M.-N.; Barreau, C.; Richard-Forget, F. *Fusarium* Response to Oxidative Stress by $H_2O_2$ Is Trichothecene Chemotype-Dependent. *FEMS Microbiol. Lett.* **2009**, *293* (2), 255−262.
(42) Salatto, D.; Huang, Z.; Benziger, P. T.; Carrillo, J.-M. Y.; Bajaj, Y.; Gauer, A.; Tsapatsaris, L.; Sumpter, B. G.; Li, R.; Takenaka, M.; Yin, W.; Thanassi, D. G.; Endoh, M.; Koga, T. Structure-Based Design of Dual Bactericidal and Bacteria-Releasing Nanosurfaces. *ACS Appl. Mater. Interfaces* **2023**, *15* (2), 3420−3432.
(43) Zorov, D. B.; Juhaszova, M.; Sollott, S. J. Mitochondrial Reactive Oxygen Species (ROS) and ROS-Induced ROS Release. *Physiol. Rev.* **2014**, *94* (3), 909−950.
(44) Krause, M.; Durner, J. Harpin Inactivates Mitochondria in *Arabidopsis* Suspension Cells. *Mol. Plant-Microbe Interact.* **2004**, *17* (2), 131−139.
(45) Garrido, C.; Galluzzi, L.; Brunet, M.; Puig, P. E.; Didelot, C.; Kroemer, G. Mechanisms of Cytochrome c Release from Mitochondria. *Cell Death Differ.* **2006**, *13* (9), 1423−1433.
(46) Ajmal, M.; Hussain, A.; Ali, A.; Chen, H.; Lin, H. Strategies for Controlling the Sporulation in Fusarium Spp. *J. Fungi* **2023**, *9* (1), 10.
(47) Le, P. H.; Nguyen, D. H. K.; Aburto-Medina, A.; Linklater, D. P.; Crawford, R. J.; MacLaughlin, S.; Ivanova, E. P. Nanoscale Surface Roughness Influences *Candida Albicans* Biofilm Formation. *ACS Appl. Bio Mater.* **2020**, *3* (12), 8581−8591.
(48) Pho, T.; Janecka, M. A.; Pustulka, S. M.; Champion, J. A. Nanoetched Stainless Steel Architecture Enhances Cell Uptake of Biomacromolecules and Alters Protein Corona Abundancy. *ACS Appl. Mater. Interfaces* **2024**, *16* (43), 58427−58438.


https://doi.org/10.1021/acsomega.4c09511
*ACS Omega* 2025, 10, 19326−19334